Mon. Not. R. Astron. Soc. **299,** 229–236 (1998)

Clustering of X-ray selected active galactic nuclei

F. J. Carrera,[1,2]★ X. Barcons,[1,3] A. C. Fabian,[3] G. Hasinger,[4] K. O. Mason,[2] R. G. McMahon,[3] J. P. D. Mittaz[2] and M. J. Page[2]

[1]*Instituto de Física de Cantabria (Consejo Superior de Investigaciones Científicas – Universidad de Cantabria), Avenida de los Castros, 39005 Santander, Spain*
[2]*Mullard Space Science Laboratory, University College London, Holmbury St. Mary, Dorking, Surrey RH5 6NT*
[3]*Institute of Astronomy, Madingley Road, Cambridge CB3 0HA*
[4]*Astrophysikalisches Institut Potsdam, An der Sternwarte 16, Potsdam, Germany*

Accepted 1998 April 28. Received 1998 April 28; in original form 1997 August 27

ABSTRACT

A total of 235 active galactic nuclei (AGN) from two different soft X-ray surveys [the *ROSAT* Deep Survey (DRS) and the *ROSAT* International X-ray Optical Survey (RIXOS)] with redshifts between 0 and 3.5 are used to study the clustering of X-ray selected AGN and its evolution. A 2σ significant detection of clustering of such objects is found on scales < 40–$80\,h^{-1}$ Mpc in the RIXOS sample, while no clustering is detected on any scales in the DRS sample. Assuming a single power-law model for the spatial correlation function (SCF), quantitative limits on the AGN clustering have been obtained: a comoving correlation length $1.5 \lesssim r_0 \lesssim 3.3\,h^{-1}$ Mpc is implied for comoving evolution, while $1.9 \lesssim r_0 \lesssim 4.8$ for stable clustering and $2.2 \lesssim r_0 \lesssim 5.5$ for linear evolution. These values are consistent with the correlation lengths and evolutions obtained for galaxy samples, but imply smaller amplitude or faster evolution than recent ultraviolet and optically selected AGN samples. We also constrain the ratio of bias parameters between X-ray selected AGN and *IRAS* galaxies to be $\lesssim 1.7$ on scales $\lesssim 10\,h^{-1}$ Mpc, a somewhat smaller value than is inferred from local large-scale dynamical studies.

Key words: surveys – galaxies: active – galaxies: clusters: general – quasars: general – large-scale structure of Universe – X-rays: general.

1 INTRODUCTION

Since the launch of *ROSAT* in 1991, a large number of surveys of soft X-ray selected sources have been undertaken using the Position Sensitive Proportional Counter (PSPC), with different sky coverages, depths and identification completenesses. They range from the *ROSAT* All Sky Survey (RASS; Voges 1992) that covers the whole sky to a fairly bright flux limit, passing through the relatively large solid angle *ROSAT* International X-ray Optical Survey (RIXOS, 20 deg^2; Mason et al., in preparation), to the deeper *ROSAT* Deep Survey (DRS; Shanks et al. 1991), Cambridge Cambridge *ROSAT* Serendipitous Survey (Boyle et al. 1995) or the UK Medium Survey (Carballo et al. 1995). The deepest and narrowest surveys, pushing to the limit the capabilities of the PSPC, are the UK Deep Survey (Branduardi-Raymont et al. 1994; McHardy et al. 1998) and the Deep Survey in the Lockman Hole (Hasinger et al. 1993, 1998; Schmidt et al. 1998).

Together, these surveys have given considerable insight into the evolution of the active galactic nuclei (AGN) X-ray luminosity function (Boyle et al. 1994; Page et al. 1996; Jones et al. 1997), their X-ray spectra (Bade et al. 1995; Carballo et al. 1995; Almaini et al. 1996; Romero-Colmenero et al. 1996; Ciliegi et al. 1997; Mittaz et al. 1998) and their relation to Narrow Emission Line Galaxies (NELGs; Boyle et al. 1995; Griffiths et al. 1996; Page et al. 1997).

However, so far the only direct study of the clustering properties of X-ray selected AGN is that by Boyle & Mo (1993, henceforth BM). They studied the local ($z < 0.2$) AGN in the Extended *Einstein* Medium Sensitivity Survey (EMSS; Stocke et al. 1991) and found no signal above 1σ, consistent with the clustering properties of the ultraviolet (UV) and optically selected AGN.

In this work we present for the first time a direct study of the clustering of soft X-ray selected AGN from *ROSAT*, using RIXOS and the *ROSAT* Deep Survey (positions and redshifts for the AGN identified in the five DRS fields have been kindly provided by O. Almaini, prior to publication).

The samples are introduced in Section 2. We discuss the evidence for clustering in Section 3, using different model-independent methods. Quantitative measurements on the correlation strength and evolution are then obtained in Section 4. These results are presented in Section 5, and discussed in Section 6. We summarize our conclusions in Section 7.

★ E-mail: carreraf@ifca.unican.es

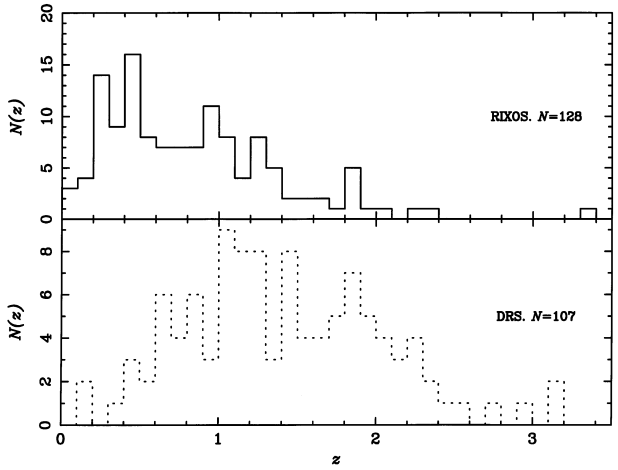

Figure 1. Histogram of the distribution of the redshifts of the AGN in RIXOS and DRS (see text).

We have used $H_0 = 100\,h$ km s^{-1} Mpc^{-1} and $q_0 = 0.5$ (unless otherwise stated) throughout this paper.

2 THE DATA

We have used two large complete soft X-ray AGN samples: DRS (Boyle et al. 1994; Shanks et al., in preparation), and RIXOS (Page et al. 1996; Mason et al., in preparation).

The DRS sample is the deepest, being a 'pencil beam' style survey in a few chosen directions in the sky, while RIXOS is wider (a collection of many shallower pencil beams), being a compromise between depth and surveyed solid angle. Both surveys together cover a wide range of redshifts (see Fig. 1) and allow an investigation of the clustering properties of X-ray AGN.

(i) *DRS*. Five deep PSPC exposures have been searched for sources down to the sensitivity limit of that instrument over the inner field of view (off-axis angle < 18 arcmin). Owing to the increasing width of the point spread function (PSF) with off-axis radius and to vignetting, the flux limit of this survey is a function of off-axis radius and different for each field. This has been taken into account in our study, as well as the fact that the source identification completeness also varies with flux (see Section 3.2). A total of 107 X-ray AGN have been detected in these fields, with redshifts between 0 and 3.5.

(ii) *RIXOS*: This is a wider solid angle shallower survey than the DRS, in which the central 17-arcmin radius solid angle of 80 medium–deep PSPC pointings with $|b| > 20°$ and exposure times longer than 8000 s have been source searched. About 90 per cent of the sources in a total of 65 fields have been identified down to a uniform limit of 3×10^{-14} erg cm^{-2} s^{-1} (0.5–2 keV), significantly higher than the sensitivity limit of all fields (Mason et al., in preparation). We have further selected those fields with an exposure time longer than 10 000 s, resulting in 43 fields (see Table 1) and 128 AGN with redshifts between 0 and 3.5.

The median luminosities of the RIXOS and DRS samples are similar: $L_{0.5-2\,\mathrm{keV}} \sim 0.2 \times 10^{44}$ erg s^{-1} (assuming a power-law spectrum with an $\alpha = 1$ energy index). The average values are however different: $\langle L_{44} \rangle \sim 0.46$ for RIXOS while $\langle L_{44} \rangle \sim 0.23$ for DRS. This indicates that, while the sources in both samples have similar overall luminosities, the luminous AGN in RIXOS are brighter than those in the DRS (see figs 2 of Boyle et al. 1994 and Page et al. 1996). We will see that this does not have any effect on our results in Section 3.2.

Table 1. RIXOS fields used. The column labelled 'RIXOS' gives the RIXOS field identification number and the column labelled '#' is the *ROSAT* sequence identification number (see Section 2).

RIXOS	#	RIXOS	#
110	200329rp	234	700112rp
115	000049rp	240	700055rp
116	000054rp	245	700099rp
122	170174rp	248	700329rp
123	700228rp	252	700319rp
125	200322rp	253	700387rp
126	700223rp	254	700391rp
205	100578rp	255	700315rp
206	200453rp	257	700326rp
211	700210rp	258	700358rp
215	150046rp	259	700010rp
216	700211rp	260	300158rp
217	700248rp	261	201103rp
219	700208rp	262	701048rp
220	701200rp	265	700216rp
221	700546rp	268	700392rp
223	200721rp	271	700510rp
224	100308rp	272	700489rp
225	200076rp	273	700384rp
226	700073rp	274	700227rp
227	200091rp	302	700540rp
228	400020rp		

Table 2. The different samples. 'N' is the number of AGN in each sample. The column labelled '%' gives the percentages of Poisson simulations with likelihood values higher than those of each sample (see Section 3.1). The column labelled 'D_c' gives an estimate of the mean comoving distance between the objects in each sample (see Section 2). The samples labelled with an asterisk are the ones used in Sections 4 and 5.

Survey	z interval	$\langle z \rangle$	N	%	D_c (h^{-1} Mpc)
RIXOS*	0.0–3.5	0.838	128	61	362
RIXOS	0.0–0.5	0.321	46	42	513
RIXOS	0.5–1.0	0.768	40	4	235
RIXOS	1.0–2.0	1.362	38	51	–
RIXOS	0.0–1.0	0.529	86	17	288
DRS*	0.0–3.5	1.425	107	–	49
DRS	0.0–1.0	0.668	27	–	161
DRS	1.0–3.5	1.680	80	–	38

The number of objects in each sample and the average redshifts for different redshift ranges are shown in Table 2. Also given are D_c, the comoving distances below which the total number of observed pairs (see Section 3.2) equals half the number of objects in the sample. This is an estimate of the mean distance between the objects in each sample, given the 'pencil beam' geometry of each of the *ROSAT* fields that make up our two surveys. D_c is missing for the RIXOS $1 < z < 2$ sample because there are only 16 pairs in total in that sample. Our default samples are those marked with an asterisk in Table 2: the total RIXOS and DRS samples, a total of 235 AGN. These two samples have complementary redshift distributions: most RIXOS AGN are at $z < 1$ ($\langle z \rangle = 0.84$), while most DRS AGN are at $z > 1$ ($\langle z \rangle = 1.43$) (see Fig. 1 and Table 2). In this sense, RIXOS reflects the 'local' behaviour of AGN clustering, while DRS can constrain its 'medium–high redshift' evolution.

3 IS THERE ANY EVIDENCE FOR CLUSTERING IN THESE SAMPLES?

We have investigated the presence of clustering in the RIXOS sample in two different model-independent ways: by comparing the distribution of the number of sources per field in each sample with that expected from a purely Poisson distribution (a variant of the counts-in-cells method, but in angular rather than spatial cells) and by comparing the total number of pairs of sources separated by a comoving distance r_c with that expected from a uniform spatial distribution of sources. This second method has also been used for the DRS sample, the first not being adequate because of the small number of fields (five) of that sample.

3.1 Counts-in-cells: checking the uniformity of our RIXOS sample

If N is the total number of AGN in a sample, n is the total number of fields ($n = 43$ for RIXOS), $\mu \equiv N/n$ is the observed average number of sources per field, and N_i is the number of sources in field i, we define a likelihood

$$L = -\sum_i \log P_\mu(N_i), \tag{1}$$

where $P_\mu(N_i)$ is the Poisson probability of finding N_i from a Poisson process of average μ

$$P_\mu(N) = \frac{\mu^N \mathrm{e}^{-\mu}}{N!}. \tag{2}$$

For each sample, 1000 Poisson simulations with the same μ, N and n as the real sample are performed, and the likelihood L is calculated for each one of them. The percentage of Poisson simulations with likelihood values larger than those of the corresponding observed samples are given in the last column of Table 2.

We can see that 96 per cent of the Poisson simulations have 'better' likelihood than the RIXOS $0.5 < z < 1$ sample or, in other words, there is evidence for clustering at the 2σ level in RIXOS in the 0.5–1 redshift interval. This is independent of the nature of the clustering.

The significance becomes smaller if we consider together all AGN with $0 < z < 1$, probably because the volume sampled at low redshift is much smaller. The lack of clustering signal in the higher redshift bin ($1 < z < 2$) is probably caused by a combination of the falling sensitivity (typical in a flux-limited survey) and the lower clustering amplitude at higher redshift ('positive evolution', see Section 5). This method does not detect any significant clustering in the whole RIXOS sample ($0 < z < 3.5$).

This test has also been used to check for possible effects of the galactic absorption and/or exposure times on the mean density of sources in different fields. We have found that there is no significant difference between the low and high column density fields, nor between the shorter and longer exposure time fields, in terms of the surface density of RIXOS sources. This test was also repeated for the faint and bright sources separately, finding the same negative result. We can thus be confident in the uniformity of our source sampling with respect to 'instrumental' selection effects.

3.2 Pairs of sources

The previous method discards all the information on the spatial separation of the sources. It is obvious that two sources in the same field, but at the opposite ends of the redshift interval, are physically unrelated. The counts-in-cells method used above does not have a way of discriminating against such cases, unless the redshift intervals are made smaller, in which case the quality of the statistics worsens.

We have performed new simulations in which as many sources as in the real samples are redistributed at random among the different fields (but not between the two different samples), keeping their redshifts and fluxes, but randomizing their off-axis angles and 'azimuths' (angle between the line joining the field centre to the source and the meridian through the field centre). This has been done in a different way for the two samples:

(i) *DRS*. In this sample, the survey effective solid angle was different for every field and a function of off-axis angle within every field (see table 2 of Boyle et al. 1994). A total of 25 different regions were defined, five for every field, corresponding to the off-axis ranges 0–10, 10–12, 12–14, 14–16 and 16–18 arcmin. The flux limit $S_{\rm lim}$ for source detection was different in each one of these 25 regions, as was the overall identification completeness for sources with $S > S_{\rm lim}$. The 'effective' solid angle $\Omega_{\rm eff}(S_{\rm lim})$ of the survey for $S > S_{\rm lim}$ is defined so that $\Omega_{\rm eff}(S_{\rm lim})/\Omega_{\rm geom}(S_{\rm lim})$ is the fraction of identified sources down to that flux limit, where $\Omega_{\rm geom}(S_{\rm lim})$ is the total solid angle surveyed, also down to the same flux limit. When a simulated source with flux S' was extracted, we found the highest $S'_{\rm lim}$ so that $S' > S'_{\rm lim}$. The source could be detected over the total surveyed area with $S_{\rm lim} \leq S'_{\rm lim}$. A particular region within that area (and hence a field) was assigned at random to the source, proportionally to $\Omega_{\rm eff}(S_{\rm lim})/\Omega_{\rm eff}(S'_{\rm lim})$. Finally, the off-axis angle and azimuth were obtained assuming a uniform source distribution within the corresponding off-axis range.

(ii) *RIXOS*. The source density is uniform within every field and field to field in this sample. Therefore, we assigned at random a RIXOS field to every source, and an off-axis angle (within 17 arcmin) and azimuth within that field.

The number $N_{\rm obs}$ of pairs of sources in the two (separate) real samples with comoving distance $\leq r_c$ is then obtained, as well as the mean number (among 100 000 simulations) of random pairs $N_{\rm P}$ up to the same separation. The distances r_c are calculated in comoving coordinates according to the expressions given by Osmer (1981), for $q_0 = 0$ and 0.5. Only pairs of sources in the same (real or simulated) field are used, to facilitate the calculation of the volume integrals introduced in Section 4.

We have used the integrated Poisson probability of obtaining $< N_{\rm obs}$ pairs for a distribution of mean μ ($= N_{\rm P}$):

$$P_\mu(< N_{\rm obs}) \equiv \sum_{N=0}^{N_{\rm obs}-1} P_\mu(N). \tag{3}$$

The complements to unity of these probabilities (i.e. $1 - P_\mu$) are plotted in Fig. 2, for the r_c values corresponding to each real pair in the RIXOS sample and the DRS sample. It is clear from this plot that there is a detection of clustering (at the ~95 per cent or 2σ level) in the RIXOS sample, at comoving distances $r_c \lesssim 40$–$80\,h^{-1}$ Mpc (e.g., $N_{\rm obs} = 22$ pairs observed for $N_{\rm P} = 14.6$ pairs expected for $r_c \leq 83.03\,h^{-1}$ Mpc). We have checked that the sources contributing to this signal are unrelated to the targets of the corresponding *ROSAT* pointings. As a general comment, the targets are mostly at $z < 0.2$ while the sources contributing to the signal have $0.2 < z < 1.4$.

It is also clear that there is not a significant detection of clustering in the DRS sample at any separation (e.g., for $r_c \leq 5.68\,h^{-1}$ Mpc, $N_{\rm obs} = 5$ and $N_{\rm P} = 4.85$). None of these results changes significantly if $q_0 = 0$ is used instead of the default $q_0 = 0.5$.

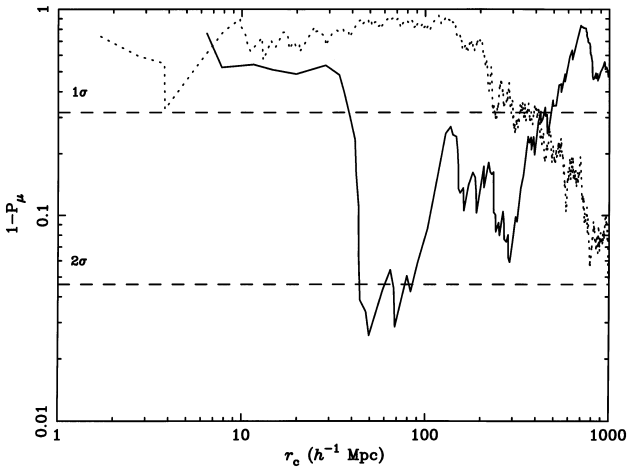

Figure 2. Complement to unity of the significance of clustering as a function of the comoving distance r_c, for the RIXOS (solid line) and the DRS AGN (dotted line). The 1σ and 2σ significance levels are shown with dashed lines

We also note the lack of significant clustering at the smallest separation of any RIXOS pairs (at $r_c \leq 6.44\,h^{-1}$ Mpc, $N_{obs} = 1$ and $N_P = 1.44$). This fact, along with the non-detection in the DRS sample at similar scales and the detection of clustering at $r_c \leq 80\,h^{-1}$ Mpc, will be used in the next section to constrain the clustering amplitude for different clustering evolution models.

The lack of very close pairs is not the result of the limited angular resolution of *ROSAT*. We have repeated the calculation of both the real and simulated pairs excluding those pairs with an angular distance smaller than 1 arcmin (larger than the minimum distance at which the *ROSAT* PSPC could resolve two separate sources at the flux levels relevant here), finding very similar results.

We have investigated if the detection of clustering in RIXOS and not in the DRS could be caused by the higher luminosity of the RIXOS sources. The average luminosity of the RIXOS sources contributing to the $r_c < 100\,h^{-1}$ Mpc pairs is $\langle L_{44}\rangle = 0.25$, while that of the DRS sources at the same separations is $\langle L_{44}\rangle = 0.24$, the median luminosities being $L_{44} = 0.17$ and $L_{44} = 0.19$, respectively. Clearly, there is no significant difference in luminosities between the two samples to which the observed difference in clustering strength could be attributed. However, there is a difference in their redshift distributions: all of the RIXOS sources at those separations are at $z < 1.4$, while most of the DRS sources have $z > 1$. This is not very surprising, considering that most models of structure formation predict the growth of inhomogeneities with cosmic time, or less clustering at higher redshift.

Finally, we would like to emphasize that this test is sensitive to all pairs with comoving separations smaller than or equal to the value of r_c shown. It is also important to stress the independence of this test on any particular clustering model.

4 THE INTEGRATED SPATIAL CORRELATION FUNCTION

Since there is an excess of AGN pairs up to a certain comoving separation, with respect to the expectation from a uniform distribution, we include now the possible spatial clustering of the sources. Indeed, the expected number of pairs up to a certain comoving separation will depend on the source correlation function integrated up to the corresponding comoving separation and taking into account the detailed geometry of the volumes sampled by the RIXOS and DRS observations.

The spatial (three-dimensional) correlation function $\xi(r)$ is defined as an excess probability (Peebles 1980). If n is the spatial density of the sources under study, the probability of finding a source in the volume dV_1 and another one in dV_2, separated by r_{12}, is:

$$\delta P = n^2[1 + \xi(r_{12})]\,dV_1\,dV_2. \tag{4}$$

As mentioned above, the relevant quantity is the integrated spatial correlation function (SCF):

$$\bar{\xi}(r_c) = \frac{1}{V}\int_V dV\xi(r), \tag{5}$$

where V is the (comoving) volume over which the pairs are counted. In the present paper, that volume is the intersection of a sphere of radius r_c with the cone defined by the maximum off-axis angles of each one of our *ROSAT* fields and the redshift limits of our samples. We assign label V_i to such volume around each of our sources with redshift z_i.

For the DRS sample, this is further refined by slicing this sphere along the conical shells defined for the different effective solid angles and flux limits for every field (see Section 3.2), and summing up the integrals over those shells, weighting them by

$$f = \frac{N(>S_{lim})}{N(>S_{min})} \times \frac{\Omega_{eff}(S_{lim})}{\Omega_{geom}(S_{lim})}, \tag{6}$$

where $N(>S)$ is the surface density of sources with flux greater than or equal to S, S_{lim} is the flux limit of the corresponding off-axis shell, S_{min} is the lowest flux limit of the DRS ($S_{0.5-2\,keV} = 0.32 \times 10^{-14}$ erg cm^{-2} s^{-1}), $\Omega_{eff}(S_{lim})$ is the effective solid angle at S_{lim}, and $\Omega_{geom}(S_{lim})$ is the total surveyed solid angle at S_{lim}. This takes into account the fraction of AGN missed by the DRS because of the different flux limits at different off-axis radii, and the fraction missed because of the flux-dependent identification incompleteness of that survey.

The expected mean number of pairs in a volume V is given by (Peebles 1980):

$$N_{exp} = N_P[1 + \bar{\xi}(r_c)]. \tag{7}$$

Given a model for the SCF, the above integrals can be performed, and the parameters of the model constrained using $P_{N\rm exp}(< N_{obs})$ (see equation 3). For example, a model with an amplitude that is too large would produce a value of N_{exp} too high compared to N_{obs} which would then be highly unlikely.

We have assumed the usual power-law shape for the SCF

$$\xi(r_c, z) = (1 + z)^{-p}(r_c/r_0)^{-\gamma}, \tag{8}$$

where r_0 is the correlation length, $\gamma = 1.8$ (the results presented below do not change significantly if $\gamma = 1.6$ is used instead) and p is an evolutionary parameter (BM). If $p = 0$ the clustering is constant in comoving coordinates ('comoving evolution'). If the clustering is constant in physical coordinates ('stable clustering') then $p = 1.2$. Linear growth of structures corresponds to $p = 2$ in an $\Omega = 1$ Universe, higher values of p representing even faster non-linear growth.

The evolution of the SCF is often parametrized, in physical coordinates, as

$$\xi(r, z) = (1 + z)^{-(3+\epsilon)}(r/r_0)^{-\gamma}, \tag{9}$$

where r is the physical distance and $\epsilon \equiv \gamma + p - 3$ (Groth & Peebles 1977).

Hence:

$$N_{\rm exp}(p, r_0) = \sum_{\Delta z} N_{\rm P}(\Delta z) \times \left(1 + \frac{r_0^{\gamma}}{N_{z_i \in \Delta z}} \sum_{z_i \in \Delta z} \frac{(1+z_i)^{(-p)}}{V_i} \int_{V_i} {\rm d}V\, r_{\rm c}^{-\gamma}\right), \quad (11)$$

where $N_{\rm P}(\Delta z)$ is the number of Poisson pairs within a redshift interval Δz ($N_{\rm P} = \sum_{\Delta z} N_{\rm P}(\Delta z)$) from the simulations. The sum $\sum_{z_i}$ is performed over all the sources with redshifts in Δz, and it is essentially an average within Δz of $\bar{\xi}(r_{\rm c})$ taking into account the clustering evolution model assumed in each case. The sum over Δz is to deal with the changing spatial density of our sources as a function of redshift, plus the geometry of our surveys and their flux limits (see Section 3.2).

We show in Fig. 3 the 'best-fit' r_0 (the value of r_0 that makes $N_{\rm exp} = N_{\rm obs}$) and the 2σ limits on r_0 for stable clustering ($p = 1.2$), as a function of $r_{\rm c}$ for the distances between each real pair of RIXOS AGN (each new point in the lines uses the cumulative distribution of pairs up to distance $r_{\rm c}$). We can see that there are only upper limits to the value of r_0 at small separations, but the required value of r_0 becomes different from zero at separations $r_{\rm c} \lesssim 40$–$80\,h^{-1}$ Mpc, in agreement with the findings of Section 3.2.

Similarly, each pair (p, r_0) can be assigned a probability for a fixed value of $r_{\rm c}$ using equations (3) and (10). This will be used in the next section to constrain the clustering of X-ray selected AGN and/or its evolution.

In Figs 2 and 3 we see that we have to go up to comoving separations of $\sim 40\,h^{-1}$ Mpc to find a significant excess of pairs with respect to an unclustered population of sources. Fig. 3 also shows that the required comoving correlation length is much smaller, so the detection of the clustering signal occurs mostly at the tails of the correlation function where clustering is weak. We do not detect an excess of pairs at comoving separations $r_c < 10\,h^{-1}$ Mpc probably because of the relatively low density of objects in our sample, in which case the number of expected pairs is always small at small separations. Although all this might seem puzzling, Fig. 3 shows that a comoving correlation length $r_0 \approx 5\,h^{-1}$ Mpc is consistent at all separations.

5 LIMITS ON THE CLUSTERING STRENGTH FOR DIFFERENT EVOLUTION MODELS

We show in Fig. 4 the 1σ, 2σ and 3σ contours in the (p, r_0) space for the distance of the closest observed pair in the RIXOS sample ($r_{\rm c} \leq 6.44\,h^{-1}$ Mpc). Since no clustering is detected at those separations, only upper limits to the value of r_0 for each p can be obtained, ranging from $r_0 \lesssim 3.8\,h^{-1}$ Mpc for comoving clustering to $r_0 \lesssim 5.5\,h^{-1}$ Mpc for linear growth (2σ).

The 1σ, 2σ and 3σ contours are plotted in Fig. 5 for the DRS AGN at $r_{\rm c} \leq 5.68\,h^{-1}$ Mpc. This distance has been chosen to represent similar scales to those in the first RIXOS pair, but, because of the absence of any signal of clustering in the DRS sample, it is representative of the whole set of distances. Only upper limits are found. They are more restrictive than those from RIXOS for $p \leq 0$, because DRS is deeper than RIXOS. Hence, it can constraint better the high-redshift behaviour of clustering ($p < 0$ implies stronger clustering at higher redshift).

The allowed region of the (p, r_0) space from the clustering signal in RIXOS is shown in Fig. 6. The comoving distance at which this is calculated ($r_{\rm c} \leq 83.03\,h^{-1}$ Mpc) is the largest one below which there is any clustering signal (at 2σ) in RIXOS, and is taken as a

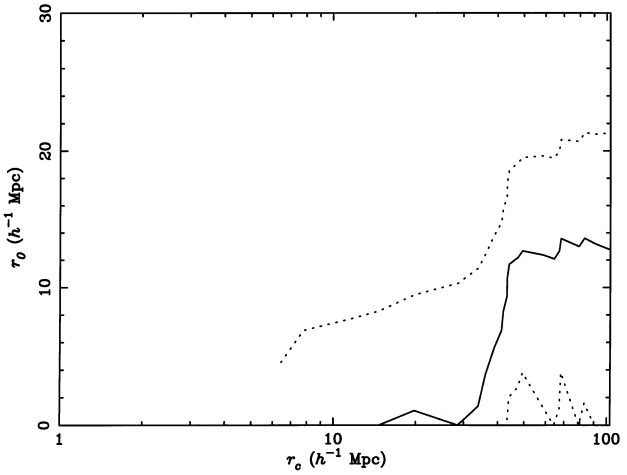

Figure 3. The 'best-fit' r_0 (solid line) as a function of the comoving separation $r_{\rm c}$ for stable clustering for the RIXOS AGN, as well as the 2σ limits (dotted lines).

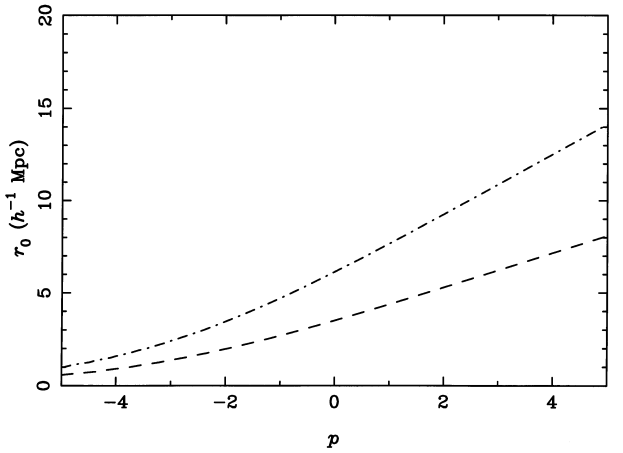

Figure 4. Probability contour levels corresponding to 1σ (solid line, confused with the p axis), 2σ (dashed line) and 3σ (dashed–dotted line) in the (p, r_0) space for the RIXOS AGN at distances $r_{\rm c} \leq 6.44\,h^{-1}$ Mpc.

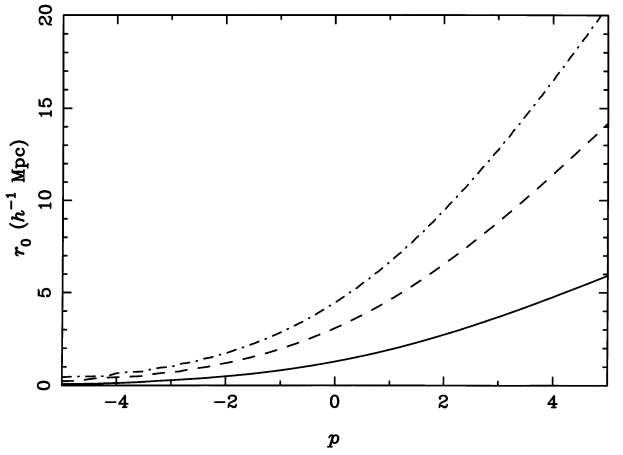

Figure 5. Probability contour levels corresponding to 1σ (solid line), 2σ (dashed line) and 3σ (dashed–dotted line) in the (p, r_0) space for the DRS AGN at distances $r_{\rm c} \leq 5.68\,h^{-1}$ Mpc.

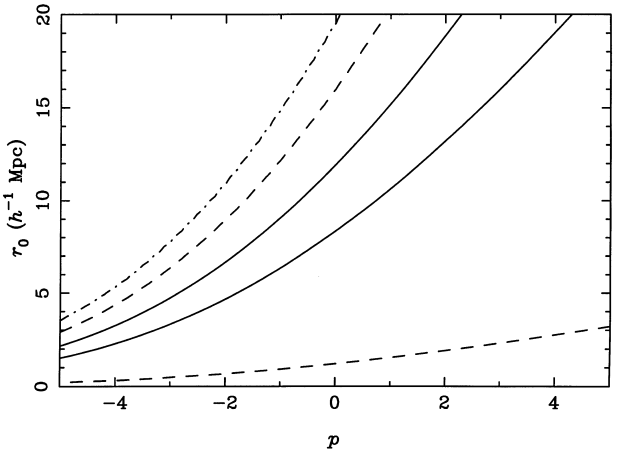

Figure 6. Probability contour levels corresponding to 1σ (solid line), 2σ (dashed line) and 3σ (dashed–dotted line) in the (p, r_0) space for the RIXOS AGN at distances $r_c \leq 83.03\,h^{-1}$ Mpc.

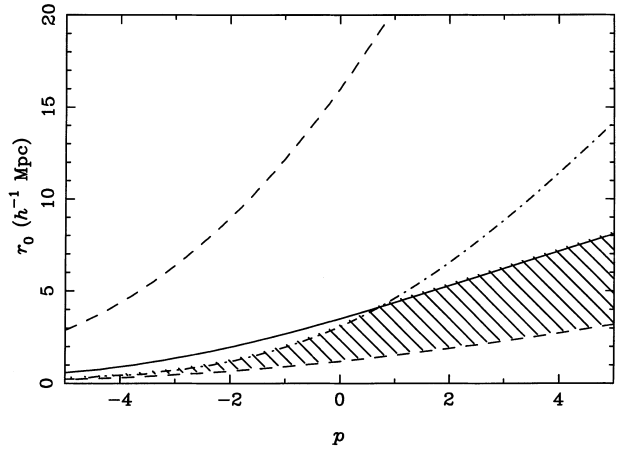

Figure 7. Probability contour levels corresponding to 2σ from RIXOS $r_c < 6.44\,h^{-1}$ Mpc (solid line) and $r_c < 83.03\,h^{-1}$ Mpc (dashed lines), and DRS $r_c < 5.68\,h^{-1}$ Mpc (dashed–dotted line). The allowed region is that below the solid and dashed–dotted lines and between the two dashed lines (shown shaded).

representative value. The value $r_0 = 0$ (no clustering) is excluded at $>2\sigma$ level for any value of p, in accordance with our detection of clustering.

Figs 4, 5 and 6 can be combined to produce a joint set of limits on the clustering strength and evolution, using the RIXOS small- and large-scale 'low-redshift' results and the DRS small-scale 'high-redshift' results. The 2σ contours from those three plots are shown in Fig. 7 together. Note that a region in the (p, r_0) parameter space 'outside' any of the 2σ contours is actually excluded at more than 2σ significance, when the three sets of contours are taken into acount simultaneously (or any combination of two of them).

To reproduce simultaneously the lack of close pairs and the clustering below $\sim 80\,h^{-1}$ Mpc in RIXOS, r_0 has to be between the lower dashed line and the solid line in Fig. 7. This translates to $1.5 \lesssim r_0 \lesssim 3.8\,h^{-1}$ Mpc for comoving evolution, $1.9 \lesssim r_0 \lesssim 4.8$ for stable clustering and $2.2 \lesssim r_0 \lesssim 5.5$ for linear evolution of clustering ($>2\sigma$ significance).

The addition of the DRS limits reduces slightly the upper limit on r_0 for the comoving evolution model: $1.5 \lesssim r_0 \lesssim 3.3\,h^{-1}$ Mpc, leaving the others unchanged.

Using $q_0 = 0$ increases the limits: comoving evolution is allowed for $2 \lesssim r_0 \lesssim 4.2\,h^{-1}$ Mpc, $2.5 \lesssim r_0 \lesssim 5.8$ for stable clustering and $2.9 \lesssim r_0 \lesssim 8.3$ for linear evolution of clustering. These are also $>2\sigma$ limits.

We have addressed the question of how much our results depend on the exact r_c value chosen to reflect the scales at which there is some signal in our RIXOS sample. We have repeated the calculations for $r_c \leq 43.96\,h^{-1}$ Mpc, the first comoving distance at which there is any signal above 2σ. They are very similar to those for $r_c \leq 83.03\,h^{-1}$ Mpc, the lower 2σ limits being $\sim$19 per cent higher. We therefore conclude that $r_c \leq 83.03\,h^{-1}$ Mpc is representative of the whole $r_c \lesssim 40$–$80\,h^{-1}$ Mpc range.

6 DISCUSSION

The clustering of galaxies seems to evolve according to the stable model or even faster with correlation lengths $r_0 \sim 3$–$7\,h^{-1}$ Mpc. Smaller correlation lengths ($r_0 \lesssim 3\,h^{-1}$ Mpc) would be required if the evolution is comoving (see e.g. Infante, de Mello & Menanteau 1996; Le Fèvre et al. 1996; Hudon & Lilly 1996; Carlberg et al. 1997; Brainerd & Smail 1998). These values are of the order of our limits for the corresponding evolution models, and therefore our results imply similar clustering properties of galaxies and X-ray selected AGN.

However, clustering of optically UV selected AGN appears to be stronger than that implied by our results. For instance, Croom & Shanks (1996) find $r_0 = 5.4 \pm 1.1\,h^{-1}$ Mpc and comoving evolution assuming a $\gamma = 1.8$ power law. Using a biasing model they obtain $r_0 \sim 7$–$8\,h^{-1}$ Mpc and slow evolution (comoving or slightly faster). These results were obtained at $r_c \leq 10\,h^{-1}$ Mpc. They are higher than our RIXOS and DRS upper limits at comparable scales.

A number of recent works have found an increase in the clustering of AGN for increasing redshift: Stephens et al. (1997) found $r_0 = 18 \pm 8\,h^{-1}$ Mpc assuming comoving clustering evolution with a sample of 56 AGN with $z > 2.7$ over $\sim$22 deg^2. This is much higher than our corresponding upper limits, and assuming evolution in comoving coordinates would lead to $p < 0$, again in conflict with our results. However, we only have five AGN with $z > 2.7$, so we essentially do not have any information at these redshifts. A clustering evolution scenario in which clustering is strong at high redshifts, then it decays, and grows again at lower redshift, would in principle be compatible with both their and our results. This is qualitatively the behaviour of the model suggested by Bagla (1998), in which higher (rarer) mass overdensities collapse early and cluster very strongly. The clustering amplitude then decreases while lower and lower mass objects collapse. When the average mass objects have collapsed, clustering starts growing again because of their mutual gravitational attraction.

La Franca, Andreani & Cristiani (1998) found a 2σ significant increase in the quasar (AGN with $M_B \leq 23$) clustering amplitude between $z = 0.95$ and $z = 1.8$ using a new sample of objects. However, if other samples are also taken into account, the significance of this decreases. In particular, if we use the four values for $\bar{\xi}(r_c \leq 15\,h^{-1}\,\mathrm{Mpc}, z)$ that are mutually independent in their work and fit $\bar{\xi}(15, z)$ to those data, $p \geq 0$ cannot be excluded at more than 75 per cent probability. The data points used in this fit are: $\bar{\xi}(15, 0.97) = 0.5 \pm 0.2$ and $\bar{\xi}(15, 1.85) = 0.8 \pm 0.3$ from La Franca et al. (1998), $\bar{\xi}(15, 0.05) = 0.2 \pm 0.3$ from BM and Georgantopoulos & Shanks (1994), and $\bar{\xi}(15, 3.1) = 1.2 \pm 0.7$ from Kundić (1997). Moreover, a 2σ effect such as the one reported by La Franca et al. (and indeed, as our own clustering detection) is not very significant and requires further work to confirm or reject it.

An interesting conclusion of our results applies to the estimates of the anisotropies introduced in the X-ray background (XRB) by source clustering. Several studies have used the angular autocorrelation function (ACF) of the X-ray background (XRB) to constrain the contribution of AGN to the XRB (Carrera & Barcons 1992; Carrera et al. 1993; Georgantopoulos et al. 1993; Danese et al. 1993; Chen et al. 1994; Sołtan & Hasinger 1994). In general, those studies coincided in stating that sources clustered on scales of 6 to $8\,h^{-1}$ Mpc with a correlation fixed in comoving coordinates could not produce more than about half of the XRB. A population of sources with a smaller correlation length or faster evolution (stable or linear) could make up the remaining XRB. These constraints are relaxed by our work, since it appears that X-ray selected AGN present weaker clustering and a faster than comoving evolution in their correlation function.

Recent soft X-ray surveys show that soft broad-line AGN only contribute ~50–60 per cent of the soft XRB, and that the contribution from harder sources (NELGs or absorbed AGN) grows at faint fluxes (Boyle et al. 1994; Page et al. 1996; Romero-Colmenero et al. 1996; Almaini et al. 1996). Whatever the ultimate nature of the hard sources turns out to be, if their clustering properties are like those of galaxies or like those of the AGN studied here, the whole soft XRB intensity could be produced by AGN and NELGs with stable or linear clustering evolution and r_0 values within the limits found here (see e.g. fig. 5 of Carrera & Barcons 1992).

It is also interesting to assess the impact of our studies on the contribution of AGN to the hard XRB. If hard X-ray AGN cluster as the soft X-ray AGN considered here, they could produce the whole hard XRB without exceeding the upper limits from the ACF (Carrera et al. 1993; Danese et al. 1993). At the moment, hard X-ray surveys only resolve a small fraction of the hard XRB (Ueda et al. 1998).

Finally, we can use our upper limits on r_0 from the smallest separation RIXOS pair to limit the ratio of bias parameters between X-ray selected AGN and *IRAS* galaxies: $b_{\rm X}/b_{\rm I} \sim \sigma_{8X}/\sigma_{8I}$, where

$$\sigma_8^2 = \frac{72(r_0/8)^{\gamma}}{2^{\gamma}(3-\gamma)(4-\gamma)(6-\gamma)} \qquad (12)$$

is the variance of the counts in a sphere of radius $8\,h^{-1}$ Mpc for a power-law clustering model, and $\sigma_{8I} = 0.69 \pm 0.04$ (Fisher et al. 1994). Our results for the three evolution models considered span $b_{\rm X}/b_{\rm I} \lesssim 0.8$–$1.7$. These upper limits are somewhat smaller than previous estimates: $b_{\rm X} \sim (6.8 \pm 1.6)\Omega^{0.6}$ from the comparison of the dipole of bright 2–10 keV selected AGN with the motion of the Local Group (Miyaji 1994), $b_{\rm X}/b_{\rm I} \sim 1.5$–$5$ from cross-correlation of those AGN with *IRAS* galaxies (Miyaji 1994), and $b_{\rm X} \approx 5.6$ from a comparison between the X-ray and microwave backgrounds (Boughn, Crittenden & Turok 1998). This difference might result from the different scales sampled. Our result applies to scales $\sim 10\,h^{-1}$ Mpc, which is where fluctuations are usually normalized, whilst the other studies measure the bias parameter on much larger scales, $\sim 1000\,h^{-1}$ Mpc. Our results are, however, similar to those of Treyer et al. (1998) ($b_{\rm X} \sim 0.9$–1.8) obtained from a study of the harmonic coefficients of the large angular scale fluctuations of the XRB from *HEAO1 A2* data.

7 CONCLUSIONS

The spatial correlation function of soft X-ray selected AGN has been studied here using data from two different X-ray surveys: the *ROSAT* Deep Survey (DRS) and RIXOS.

Some indication of clustering at the 2σ level in RIXOS in the $z = 0.5$–1 redshift range has been found using a variant of the counts-in-cells method. A more powerful test has also been performed, by comparing the number of pairs of sources in each sample with the number of pairs expected from a uniform distribution of sources, finding a $\sim 2\sigma$ significant clustering signal in the whole RIXOS sample ($\langle z \rangle = 0.53$) in comoving scales $r_{\rm c} \lesssim 40$–$80\,h^{-1}$ Mpc. No significant detection has been found in the DRS sample ($\langle z \rangle = 1.4$) or in the RIXOS sample at small scales. Both tests are model-independent.

Quantitative measurements of the clustering and its evolution have been obtained from the integrated spatial correlation function (essentially the number of pairs with comoving separations smaller than or equal to $r_{\rm c}$), assuming Poisson statistics, and a power-law shape for the correlation function, with slope $\gamma = 1.8$ and correlation length r_0.

Combining the limits from RIXOS ($r_{\rm c} \lesssim 6\,h^{-1}$ Mpc and $r_{\rm c} \lesssim 80\,h^{-1}$ Mpc) with the DRS limits ($r_{\rm c} \lesssim 6\,h^{-1}$ Mpc), we obtain: $1.5 \lesssim r_0 \lesssim 3.3\,h^{-1}$ Mpc for comoving clustering, $1.9 \lesssim r_0 \lesssim 4.8$ for stable clustering and $2.2 \lesssim r_0 \lesssim 5.5$ for linear evolution of clustering. Using $q_0 = 0$ we obtain ~20–30 per cent higher limits.

These results are compatible with the clustering properties of 'normal' galaxies, but would imply weaker clustering in X-ray selected AGN than in optically UV selected ones. Our results do not support an increase in the clustering amplitude with redshift. However, we do not have many sources above $z > 2.5$, so we cannot rule out nor support the strong clustering above that redshift found by Stephens et al. (1997).

AGN (and/or NELGs) clustered like the sources studied here could produce most of the hard and soft X-ray background without exceeding the observed limits on its autocorrelation function.

The lack of very close pairs in RIXOS implies that the ratio of bias parameters between X-ray selected AGN and *IRAS* galaxies (where there is evidence that biasing is small, $b_{\rm I} \approx 1$) is $b_{\rm X}/b_{\rm I} \lesssim 0.8$–$1.7$, somewhat smaller than previous results.

A 3σ detection at comoving separations $r_{\rm c} \lesssim 10\,h^{-1}$ Mpc would necessitate ~100–110 'RIXOS-like' fields for comoving evolution and $r_0 = 6\,h^{-1}$ Mpc. This is especially relevant for future X-ray survey identification programmes (such as the *XMM* XID) with a view to detect AGN clustering. It is much more efficient to use a compact connected area (circular or elongated) for this purpose, rather than serendipitous pointings distributed all over the sky. In this sense, the *ROSAT* All Sky Survey identification programmes will be very useful to provide a local 'anchor' for X-ray AGN clustering studies (e.g. Zickgraf et al. 1998).

ACKNOWLEDGEMENTS

Special thanks are due to Omar Almaini and his colleagues for providing us with the positions, fluxes and redshifts of the DRS AGN. FJC and XB thank the DGES for financial support, under project PB95-0122. XB acknowledges sabbatical support at Cambridge to the DGES under grant PR95-490. ACF and RGM thank the Royal Society for support. This research has made use of data obtained from the Leicester Database and Archive Service at the Department of Physics and Astronomy, Leicester University, UK. We thank the Royal Society for a grant to purchase equipment essential to the RIXOS project.

REFERENCES

Almaini O., Shanks T., Boyle B. J., Griffiths R. E., Roche N., Stewart G. C., Georgantopoulos I., 1996, MNRAS, 282, 295

Bade N., Fink H. H., Engels D., Voges W., Hagen H.-J., Wisotzki L., Reimers D., 1995, A&AS, 110, 469
Bagla J. S., 1998, MNRAS, 297, 251
Boughn S. P., Crittenden R. G., Turok N. G., 1998, New Astron., 3, 275
Boyle B. J., Mo H. J., 1993, MNRAS, 260, 925 (BM)
Boyle B. J., Shanks T., Georgantopoulos I., Stewart G. C., Griffiths R. E., 1994, MNRAS, 271, 639
Boyle B. J., McMahon R. G., Wilkes B. J., Elvis M., 1995, MNRAS, 272, 462
Brainerd T. G., Smail I., 1998, ApJ, 494, 137
Branduardi-Raymont G. et al., 1994, MNRAS, 270, 947
Carballo R., Warwick R. S., Barcons X., González-Serrano J. I., Barber C. R., Martínez-González E., Pérez-Fournon I., Burgos J., 1995, MNRAS, 277, 1312
Carlberg R. G., Cowie L. L., Songaila A., Hu E. M., 1997, ApJ, 484, 538
Carrera F. J., Barcons X., 1992, MNRAS, 257, 507
Carrera F. J., et al., 1993, MNRAS, 260, 376
Chen L.-W., Fabian A. C., Warwick R. S., Branduardi-Raymont G., Barber C. R., 1994, MNRAS, 266, 846
Ciliegi P., Elvis M., Wilkes B. J., Boyle B. J., McMahon R. G., 1997, MNRAS, 284, 401
Croom S. M., Shanks T., 1996, MNRAS, 281, 893
Danese L., Toffolatti L., Franceschini A., Martín-Mirones J. M., De Zotti G., 1993, ApJ, 412, 56
Fisher K. B., Davis M., Strauss M. A., Yahil A., Huchra J., 1994, MNRAS, 266, 50
Georgantopoulos I., Shanks T., 1994, MNRAS, 271, 773
Georgantopoulos I., Stewart G. C., Shanks T., Griffiths R. E., Boyle B. J., 1993, MNRAS, 262, 619
Griffiths R. E., Della Ceca R., Georgantopoulos I., Boyle B. J., Stewart G. C., Shanks T., Fruscione A., 1996, MNRAS, 281, 71
Groth E. J., Peebles P. J. E., 1977, ApJ, 217, 385
Hasinger G., Burg R., Giacconi R., Hartner G., Schmidt M., Trümper J., Zamorani G., 1993, A&A, 275, 1
Hasinger G., Burg R., Giacconi R., Schmidt M., Trümper J., Zamorani G., 1998, A&A, 329, 482
Hudon J. D., Lilly S. J., 1996, ApJ, 469, 519
Infante L., de Mello D. F., Menanteau F., 1996, ApJ, 469, L85
Jones L. R. et al., 1997, MNRAS, 285, 547
Kundić T., 1997, ApJ, 482, 631
La Franca F., Andreani P., Cristiani S., 1998, ApJ, 497, 529
Le Fèvre O., Hudon D., Lilly S. J., Crampton D., Hammer F., Tresse L., 1996, ApJ, 461, 534
McHardy I. M. et al., 1998, MNRAS, 295, 641
Mittaz J. P. D. et al., 1998, MNRAS, submitted
Miyaji T., 1994, PhD thesis, Univ. Maryland
Osmer P. S., 1981, ApJ, 247, 762
Page M. J. et al., 1996, MNRAS, 281, 579
Page M. J., Mason K. O., McHardy I. M., Jones L. R., Carrera F. J., 1997, MNRAS, 289, 693
Peebles P. J. E., 1980, The Large Scale Structure of the Universe. Princeton Univ. Press, Princeton, NJ
Romero-Colmenero E., Branduardi-Raymont G., Carrera F. J., Jones L. R., Mason K. O., McHardy I. M., Mittaz J. P. D., 1996, MNRAS, 282, 94
Schmidt M. et al., 1998, A&A, 329, 495
Shanks T., Georgantopoulos I., Stewart G. C., Pounds K. A., Boyle B. J., Griffiths R. E., 1991, Nat, 353, 315
Sołtan A., Hasinger G., 1994, A&A, 288, 77
Stephens A. W., Schneider D. P., Schmidt M., Gunn J. E., Winberg D. H., 1997, AJ, 114, 41
Stocke J. T., Morris S. L., Gioia I. M., Maccacaro T., Schild R., Wolter A., Fleming T. A., Henry J. P., 1991, ApJS, 76, 813
Treyer M., Scharf C., Lahav O., Jahoda K., Boldt E., Piran T., 1998, ApJ, submitted (astro−ph/9801293)
Ueda Y. et al., 1998, Nat, 391, 866
Voges W., 1992, in Proc. European International Space Year Meeting, ESA ISY-3, 9
Zickgraf F. J. et al., 1998, AN, 319, 42

This paper has been typeset from a $\TeX$/$\LaTeX$ file prepared by the author.